Available online at www.sciencedirect.com
ScienceDirect
Trans. Nonferrous Met. Soc. China 33(2023) 2044−2053
Transactions of Nonferrous Metals Society of China
www.tnmsc.cn

Effect of MgF_2 coating on stress corrosion cracking behavior of Mg−Zn−Ca alloy in simulated body fluid

Yu-feng LI[1,2], Bo-wen WANG[1], Xiao-hao SUN[3], De-bao LIU[4]

1. School of Materials Science and Engineering, Tianjin University of Technology, Tianjin 300384, China;
2. School of Materials Science and Engineering, Hebei University of Technology, Tianjin 300401, China;
3. Tianjin Key Laboratory for Photoelectric Materials and Devices, Tianjin 300384, China;
4. National Demonstration Center for Experimental Function Materials Education, Tianjin University of Technology, Tianjin 300384, China

Received 14 February 2022; accepted 1 May 2022

Abstract: The stress corrosion cracking behavior of Mg−3wt.%Zn−0.2wt.%Ca (MZC) alloy and fluoride (MgF_2) coated Mg−3wt.%Zn−0.2wt.%Ca alloy (MZC-MF) for bone implant applications was investigated using slow strain-rate tensile (SSRT) tests in simulated body fluid (SBF). The results show that MgF_2 coating could significantly improve the corrosion resistance and prolonged fracture failure time of MZC alloy. MgF_2 coating also greatly reduced the stress corrosion cracking sensitivity of MZC alloy in SBF. Compared to MZC alloy, stress corrosion cracking sensitivity index (I_{scc}) of MZC-MF alloy decreased by 21% (ultimate tensile strength, UTS), 22% (time to failure, t_f), 23% (elongation after fracture, δ), 7% (reduction ratio of cross-sectional area after fracture, φ) and 15% (inner product work, A), respectively.
Key words: Mg−Zn−Ca alloy; MgF_2 coating; stress corrosion sensitivity; stress corrosion cracking; fracture failure mode

1 Introduction

Magnesium (Mg) alloys are attracting significant attention for their potential application as temporary biodegradable implants due to good biocompatibility, mechanical compatibility, promotion of osteogenic function, and antibacterial function.

However, the disadvantages are that the chemical properties of Mg alloy are active causing the degradation rate to be too fast, which is difficult to meet the clinical requirements [1,2]. It should be noted that during the service process, the implanted device will inevitably be affected by the physiological load from the surrounding environment [3−5]. For example, the cardiovascular stent not only bears the shear stress produced by blood flow but also is subject to the cyclic load caused by the beating of the heart [2]. The synergistic effect of load and physiological corrosion medium will lead to stress corrosion cracking (SCC) [2,6,7] or corrosion fatigue (CF) [8,9] of Mg alloy. At present, many studies on the stress corrosion cracking behavior of magnesium alloys have been focused on alloys containing aluminum or heavy rare earth, which are known neurotoxic or hepatotoxic elements, and the stress corrosion cracking test has been conducted in 3 wt.% NaCl solution or distilled water. Among various Mg-based alloy systems, Mg−Zn−Ca alloy has advantages in biocompatibility, mechanical properties, and corrosion resistance [10−12]. However, according to the reports, Mg−Zn−Ca alloys exhibited greater SCC sensitivity than the commercial AZ91D alloy [2,13,14]. CHOUDHARY

Corresponding author: De-bao LIU, Tel: +86-15122966960, E-mail: debaoliu@126.com
DOI: 10.1016/S1003-6326(23)66242-9

and RAMAN [14] investigated the stress corrosion cracking behavior of AZ91D alloy and Mg−3wt.%Zn−1wt.%Ca magnesium alloy in the physiological environment using a slow strain rate tensile test (SSRT). The results show that the Mg−3Zn−1Ca alloy is more prone to stress corrosion cracking than the AZ91D alloy at a certain strain rate, which may be attributed to the fact that the Mg−3Zn−1Ca alloy is more prone to pitting and localized corrosion than the AZ91D alloy.

It is reported that surface coating can improve stress corrosion resistance. For example, JAFARI et al [15] reported that common hydroxyapatite (HAp) coating containing multi-walled carbon nanotubes (MWCNT) was applied on AZ31 Mg alloy and the slow strain rate test (SSRT) was used to study the stress corrosion resistance of Mg alloy in simulated body fluid (SBF). The results showed that the SCC sensitivity of AZ31 Mg alloy decreased from 26.8% of HAp coating to 9.8% of HAp/MWCNT coating. MgF_2 coating was widely used in the anticorrosion of medical Mg alloy because of its non-toxic, chemical inert, and simple preparation process. COOPER et al [16] reported that MgF_2 coating can significantly improve the corrosion resistance of Mg alloy and induce osteoblast proliferation. According to the results of LI et al [17], MgF_2-coated screws have good corrosion resistance in vivo and in vitro, especially in the early implanted stage. However, to the best of our knowledge, studies on MgF_2 coating has been mainly focused on its degradation behavior in the stress-free state of the simulated physiological environment, and scant reports are available exploring the influence of MgF_2 coating on the stress corrosion resistance of medical Mg alloy. Thus, it is necessary to understand the effect of stress on the degradation behavior of magnesium alloy with coating, such as stress corrosion cracking sensitivity and fracture failure mode.

In this study, MgF_2 coating was prepared on the surface of Mg−3wt.%Zn−0.2wt.%Ca (MZC) alloy. Microstructure, mechanical performance, corrosion behavior, stress corrosion cracking sensitivity, and fracture failure mode of MgF_2-coated Mg−Zn−Ca alloy were systematically investigated. This research could provide an SCC experimental foundation for the development of MgF_2-coated Mg alloy for orthopedic applications.

2 Experimental

2.1 Materials preparation

High-purity magnesium ingots (99.99 wt.%), pure zinc granules (99.99 wt.%), and magnesium−calcium intermediate alloy (25 wt.% Ca) were used as raw materials. As-cast Mg−3wt.%Zn−0.2wt.%Ca alloy was prepared by vacuum melting and was extruded into a sheet at 593 K with the extrusion ratio of 13:1. The extrusion speed was 2 mm/s.

A plate tensile specimen was machined with the dimensions shown in Fig. 1. For the electrochemical corrosion test, the rectangular specimen with a size of 10 mm × 10 mm × 3 mm was cut from the extruded sheet, and ground up to 3000 grits with SiC sandpaper.

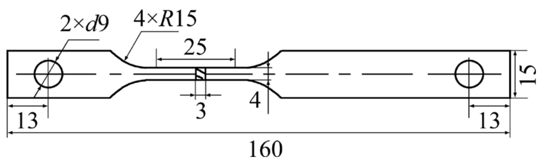

Fig. 1 Dimensions of SSRT test specimen (unit: mm)

2.2 Coating preparation and characterization

During the HF coating process, the specimen was immersed in a 20% hydrofluoric acid solution with a ratio of 25 mL/cm^2 at 310 K in a water bath for 6 h, and then rinsed with deionized water three times and dried. The MZC alloy after fluorination treatment is denoted as MZC-MF and optical image is shown in Fig. 2.

Fig. 2 Optical image of MgF_2-coated MZC alloy

A scanning electron microscope (Quanta FEG 250, FEI, USA) with an energy dispersive spectroscopy (X-act one, Oxford, UK) was utilized to observe and analyze the surface and cross-sectional morphology as well as the composition of MgF_2 coating. The phase constitutions of the coating were characterized by X-ray diffraction (XRD, Rigaku D/max/2500PC) with a step size of 0.02° and a dwelling time of 1 s.

2.3 Electrochemical measurements

According to ASTM-G 102—2015, electrochemical measurements were carried out in the SBF solution (with the composition of SBF given in Table 1) by an electrochemical workstation (Zennium, Zahner, Germany) with a standard three-electrode system (graphite as the control electrode, saturated calomel electrode as the reference electrode and the specimen as the working electrode). The working electrodes were MZC specimens and MZC-MF specimens, respectively, and the exposed area is 1 cm^2 in the solution. After the open circuit potential was recorded for 1800 s, the potential dynamic polarization was performed at a scanning rate of 1 mV/s. The voltage range was set as self-corrosion potential ±500 mV. The Tafel curve was fitted by the Tafel extrapolation method to obtain the corrosion potential (φ_{corr}) and corrosion current density (J_{corr}).

Table 1 Chemical composition of SBF

Ingredient	Content/($g\cdot L^{-1}$)
NaCl	6.5453
$NaHCO_3$	2.2683
KCl	0.3728
$Na_2HPO_4\cdot 7H_2O$	0.2681
$MgCl_2\cdot 6H_2O$	0.3050
$CaCl_2\cdot 2H_2O$	0.3676
Na_2SO_4	0.0711
$(CH_2OH)_3CNH_2$	6.0570

2.4 Slow strain-rate tensile (SSRT) tests

SSRT tests were used to determine the stress corrosion sensitivity (SCC) of MZC and MZC-MF specimens in air and SBF, respectively. According to ASTM-G 129—Y2021, plate tensile specimens with gauge dimensions of 25 mm (length), 4 mm (width), and 3 mm (thickness) were tested under a nominal strain rate of $6.7\times10^{-7}\,s^{-1}$ using a mechanical test system (DDL−020−050, Sinotest, China). The schematic diagram of the device is shown in Fig. 3. To gain a constant surface area exposure and avoid micro-galvanic corrosion with other components in the solution, the rest of the specimen beside the gauge section was wrapped with 704 silicone rubber. After the test, the fracture surface was cleaned with chromic acid and then was observed with a scanning electron microscope. Otherwise, at least three replicate specimens were tested to ensure the accuracy of the experimental data. The SCC sensitivity index (I_{SCC}) was calculated using Eq. (1) [18,19]:

$$I_{scc} = (1 - X/X_0)\times 100\% \tag{1}$$

where X represents ultimate tensile strength (UTS), time to failure (t_f), elongation after fracture (δ), reduction ratio of the cross-sectional area after fracture (φ), or inner product work (A) in SBF, and X_0 represented above five parameters in air. These five parameters were selected to fully understand the stress corrosion behavior of Mg alloy in a corrosion environment, especially, inner product work. Its physical meaning is the area enclosed by the stress−strain tensile curve of the material and the abscissa, which is obtained by the integration method. The value of I_{SCC} was in the range of 0−1, and the higher value expressed the greater sensitivity to SCC.

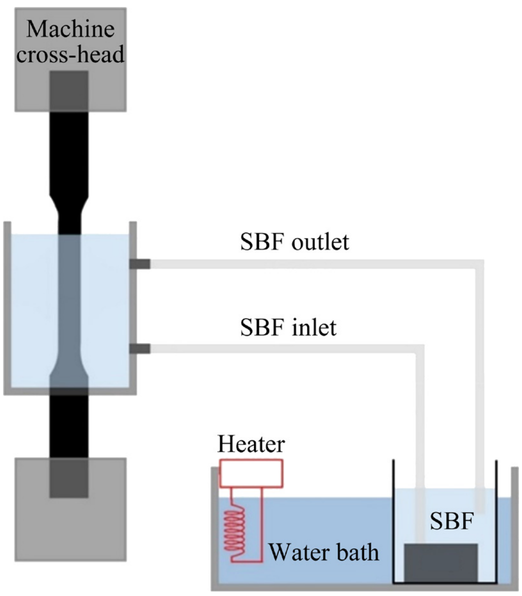

Fig. 3 Schematic diagram of SSRT test device

After the fracture of the specimens through the SSRT test, the concentration of Mg^{2+} in different corrosion media was detected. 15 mL corrosion medium was taken out for the determination of

Mg^{2+} concentration by inductively coupled plasma optical emission spectroscope (ICP-OES, Vista-MPX, Thermo Scientific, USA). The calculation formula of corrosion rate ($\overline{V}_C$) is as follows [20]:

$$\overline{V}_C = \frac{C_{Mg} \cdot V}{S \cdot t} \tag{2}$$

where C_{Mg} represents the Mg^{2+} concentration; V represents the volume of corrosion medium; S represents the surface area of the SSRT specimen exposed to the solution and t represents the exposure time in solution.

3 Results and discussion

3.1 Coating characterization

Figure 4(a) displays the surface microstructure of MZC specimens. Some large grains with strip shapes were distributed in the matrix, indicating that the dynamic recrystallization of the alloy was not complete maybe due to the smaller extrusion ratio. Figure 4(b) displays the line scanning of the MgF_2 coating, which revealed that the average coating thickness was around 2 mm. Figure 4(c) shows the MgF_2 coating microtopography. It could be seen that a small number of irregular pores and micro-crack were formed on the surface of the MgF_2 coating, and spot scanning of the MgF_2 coating as shown in Fig. 4(d) revealed that the existing elements were mainly Mg, F, O, and C. The following reaction occurred on the MZC alloy surface during the fluorination process [21]:

$$Mg+2HF \cdot H_2O \rightarrow MgF_2(s)+H_2(g)+H_2O \tag{3}$$

XRD pattern of the MgF_2 coating is shown in Fig. 5, which revealed that the MgF_2 coating was mainly composed of the MgF_2 phase. Combined with Fig. 4(c), EDS analysis showed that the atomic ratio of F element to Mg element was less than 2. The presence of carbon and oxygen may come from the hydrocarbons in the air, but part of the oxygen may derive from the aqueous solution of hydrofluoric acid. It was possibly speculated that there was some $Mg(OH)_2$ in the MgF_2 coating. VERDIER et al [22] believed that oxygen may come from hydroxide, and MgF_2 coating was a mixture of $Mg(OH)_2$ and MgF_2.

3.2 Electrochemical properties

The dynamic potential polarization curves of MZC specimens and MZC-MF specimens in SBF are shown in Fig. 6. Electrochemical data, including self-corrosion potential (φ_{corr}), self-corrosion current density (J_{corr}), and polarization resistance (R_p), were measured by Tafel extrapolation of anode and cathode polarization lines, as listed in Table 2. The

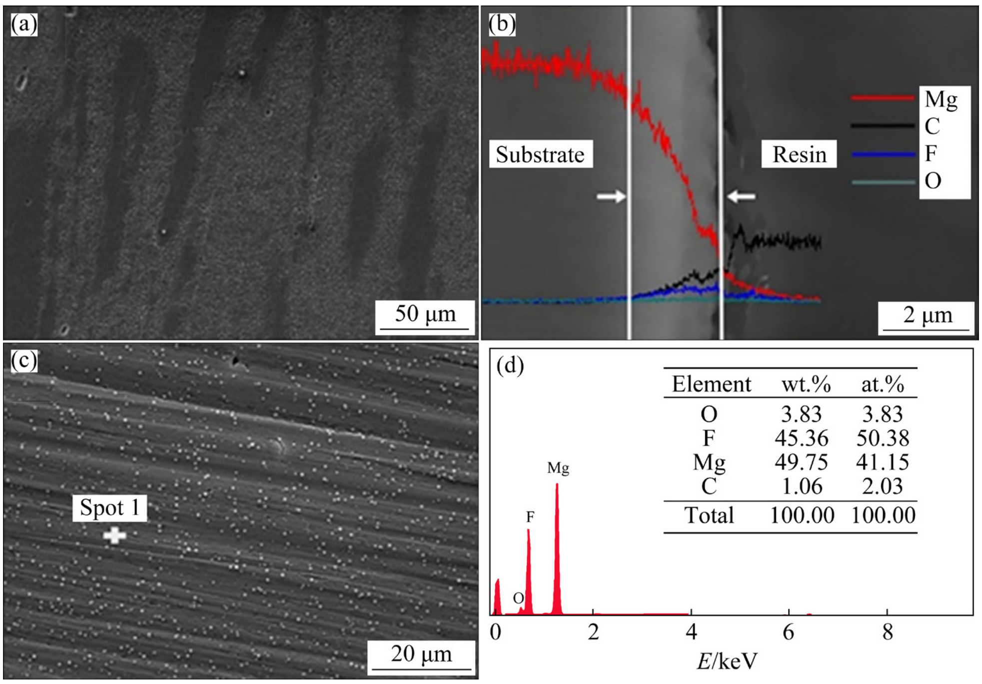

Fig. 4 SEM image showing surface microstructure of MZC alloy (a), EDS line scanning of cross-section of MZC-MF specimens (b), surface topography (c), and EDS spectrum of white point of MgF_2 coating (d)

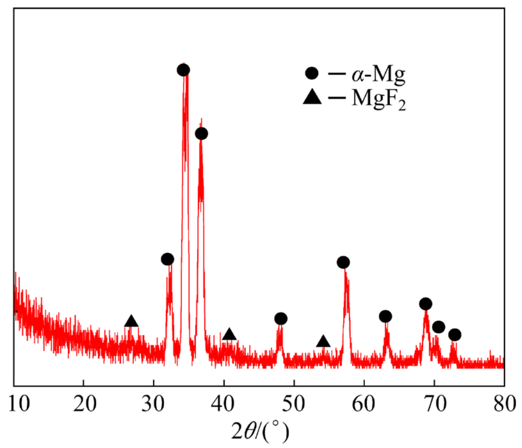

Fig. 5 XRD pattern of MgF_2 coating

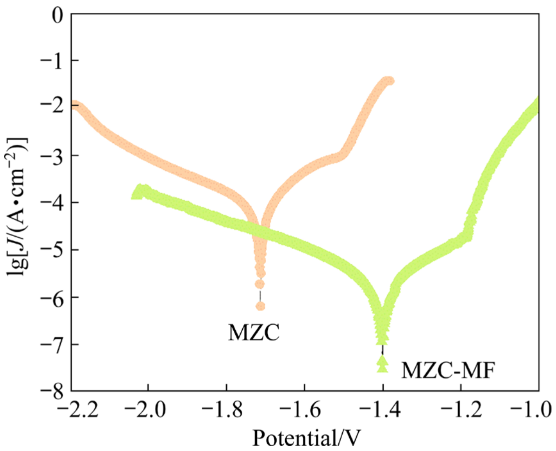

Fig. 6 Potentiodynamic polarization curves of MZC specimens and MZC-MF specimens in SBF

Table 2 Electrochemical parameters derived from polarization curves

Specimen	φ_{corr}/V	J_{corr}/(A·cm^{-2})	R_p/(kΩ·cm^{-2})
MZC	−1.72	8.85×10^{-4}	2.33
MZC-MF	−1.40	2.75×10^{-5}	96.73

cathodic polarization curve represents the evolution of cathodic hydrogen reduction by water, while the anode curve represents the anodic dissolution of Mg [23]. As can be seen from Fig. 6, the overall shape of the polarization curve was not changed, which manifested that the coating did not affect the corrosion mechanism of the MZC alloy. Furthermore, the φ_{corr} of MZC-MF specimens in SBF was increased by 0.32 mV. The positive shift of φ_{corr} means that the thermodynamic tendency of electrochemical corrosion is reduced. Higher corrosion potential and a lower corrosion current density represent a lower corrosion rate [24,25]. Compared to bare alloys, the J_{corr} was decreased by an order of magnitude, from 8.85×10^{-4} to 2.75×10^{-5} A/cm^2. These results clearly showed that the MgF_2 coating greatly improved the corrosion performance of the MZC alloy. Although SBF contains a variety of anions, such as HCO_3^-, SO_4^{2-}, and Cl^-, the presence of these ions increases the possibility of corrosion of the Mg alloy [8]. The dense and chemically stable MgF_2 coating effectively acts as a barrier to block corrosive ions from contacting the Mg matrix. The increase in corrosion resistance would greatly reduce the initial corrosion rate of the implant. It is of important significance in maintaining sufficient mechanical strength in the early stage of bone tissue healing and delaying the premature loss of mechanical properties in the late implantation period.

3.3 Stress corrosion cracking behavior

Figure 7 shows the stress−strain curve of the SSRT test in air and SBF for MZC and MZC-MF specimens. It can be seen that the mechanical properties of the MZC alloy dropped sharply in the corrosive environment compared with those in the air. The tensile curve of MZC specimens in SBF had a fracture failure before the yield point, and the mechanical attenuation of MZC-MF specimens occurred after the yield point. Table 3 gives the SSRT results of MZC and MZC-MF specimens in air and SBF.

The stress corrosion cracking sensitivity index (I_{scc}) of the UTS, t_f, δ, φ, and A is shown in Fig. 8, according to Table 3. For the specimens with lower SCC sensitivity, the I_{scc} value is lower. On the

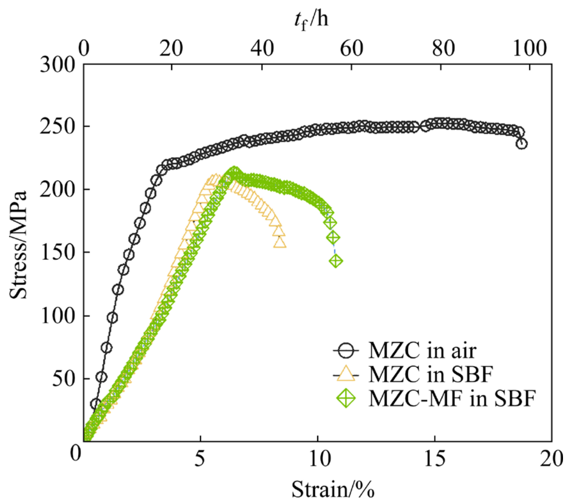

Fig. 7 Stress−strain curves of SSRT tests for different specimens in air and SBF

Table 3 SSRT results of MZC alloy with and without MgF_2 coating

Specimen	UTS/MPa	t_f/h	δ/%	φ/%	A/(10^6J·m^{-3})
MZC in air	253.25±4.15	93.78±6.52	18.60±1.41	16.37±1.45	4137.00±358.23
MZC in SBF	206.20±6.72	47.67±6.36	8.20±0.62	5.14±0.53	1075.39±135.54
MZC-MF in SBF	214.20±5.84	57.80±4.17	10.50±0.50	5.90±0.45	1527.36±146.33

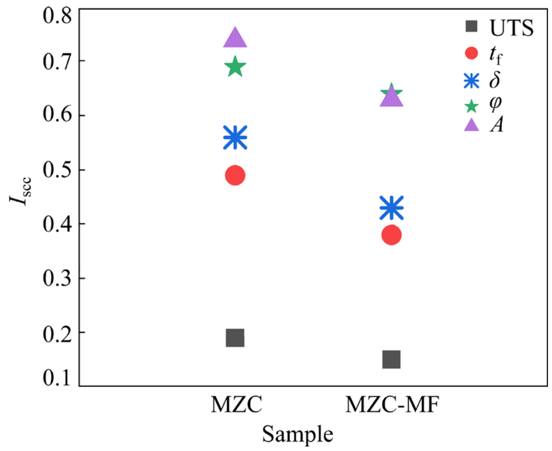

Fig. 8 Variation of I_{scc} (described in terms of UTS, t_f, δ, φ, and A)

contrary, the I_{scc} value tends to be 1, meaning higher SCC sensitivity. It can be seen from Fig. 8 that the presence of magnesium fluoride decreases the SCC sensitivity of MZC alloy. In this work, the MgF_2 coating is dense and closely combined with the matrix, which can greatly delay the crack initiation and extension during the service process. Therefore, MZC-MF alloy exhibited lower stress corrosion susceptibility index compared to the specimen reported in Refs. [14,26].

After the fracture of the specimens through the SSRT test, the concentration of Mg^{2+} in different corrosion media was detected, as listed in Table 4. According to the Mg^{2+} concentration in the solution, the average corrosion rate ($\overline{V}_C$) in different corrosive environments was calculated in Fig. 9. Because of the existence of a certain concentration of Mg^{2+} (about 34.92 mg/L tested by ICP-OES) in SBF, the calculation of $\overline{V}_C$ needs to deduct. In SBF, MZC-MF specimens had a lower $\overline{V}_C$ than MZC specimens. The existence of magnesium fluoride prolonged the fracture time of the MZC alloy in a corrosive environment and increased the corrosion resistance.

From the above analysis, the MgF_2 coating could reduce the SCC sensitivity of the MZC alloy, so it was necessary to analyze the fracture morphology of the specimens in detail. The typical

Table 4 Mg^{2+} concentration of MZC and MZC-MF specimens in SBF after SSRT fracture (mg/L)

SBF	MZC	MZC-MF
34.92	53.75±5.12	43.24±3.51

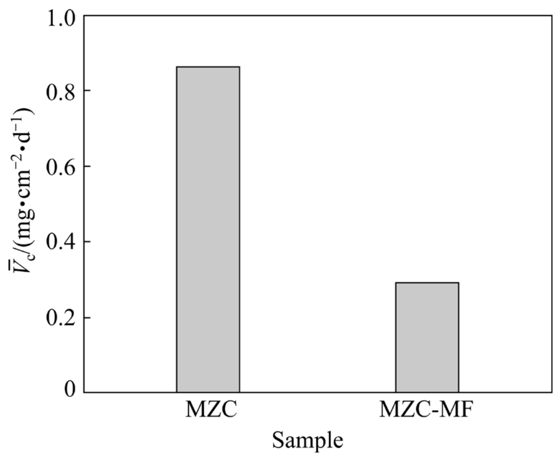

Fig. 9 Average corrosion rate of MZC specimens and MZC-MF specimens in SBF after SSRT fracture

fracture morphologies of different specimens after SSRT in air and SBF are shown in Fig. 10. It is shown that during the SSRT test of MZC specimens in air, a small part of cleavage surface and dimple were observed on the fracture surface, indicating ductile and brittle mixed fracture morphology, as shown in Figs. 10(a−c). However, in SBF, it is observed that fracture surface was relatively flat, as shown in Figs. 10(d, f). At high magnification, the fracture surface showed a transgranular fracture and secondary crack, which belongs to brittle fracture (Figs. 10(d, e)). Also, high magnification of the corrosion position showed that there were many corrosion holes around the white particles (Fig. 10(e)), which was related to the micro galvanic corrosion between the second phase and the Mg matrix. Otherwise, there were some big corrosion pits around the fracture. Pitting was considered to be the most common inducement of stress corrosion cracking of magnesium alloy [27]. Fracture analysis confirmed that the bare MZC alloy had significant stress corrosion cracking in the

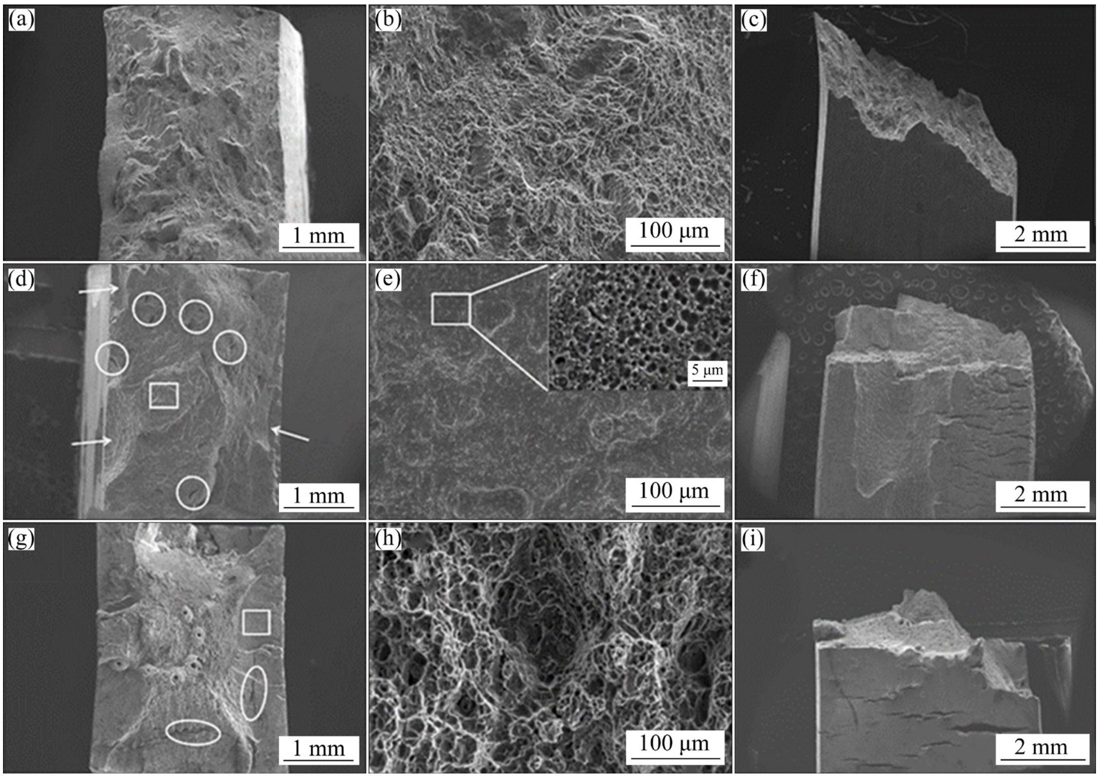

Fig. 10 Fracture characteristics of MZC specimens and MgF_2-MF specimens for SSRT in air ((a−c)), in SBF (bare MZC alloy (d−f); MgF_2 coated alloy (g−i)) (White circle indicates corrosion secondary crack, the arrow indicates the corrosion pit, and the white box indicates local amplification)

corrosion solution, and the hydrogen embrittlement (HE) effect may be the main reason for the strength and plasticity loss of the specimens. However, there were also corrosion cracks and corrosion pits on the fracture surface of the coating specimens, but the number was reduced, especially in SBF (as shown in Figs. 10(g, i)). Figure 10(h) shows the partially enlarged image of removing corrosion products in Fig. 10(g). The images showed that the corrosion was still dominated by pitting, indicating that the MgF_2 coating did not change the corrosion mode of the MZC alloy.

The fracture characteristics of the SSRT test showed that the corrosion pits caused by local corrosion or galvanic corrosion were the common stress concentration points. It was the main cause of SCC crack initiation (as shown in Figs. 10(d, g)) with several cracks that were perpendicular to the direction of application protruding in white arrows.

The fracture morphology and EDS analysis of MZC-MF specimens as shown in Fig. 11, mainly contained Ca, P, Mg, O, and other trace elements, indicating that the structure was mainly composed of $Mg(OH)_2$ and Ca−P precipitates. It may be deduced that the deposited and loose $Mg(OH)_2$ and Ca−P precipitates cannot completely prevent the reaction between the solution and the Mg [28], and the release of gas accumulated to a certain extent to break through the binding of the film, which proves that hydrogen assisted fracture is the main failure mechanism of the coating specimens.

In the early stage of SCC, the MgF_2 coating is closely combined with the substrate, which can inhibit the corrosion. Under the action of stress, the matching degree between the dense coating and the substrate gradually decreases, promoting the growth of microcracks, and leading to the increase of galvanic corrosion. Therefore, the dissolution of anode makes the mechanical strength of the specimens decrease. At the same time, part of the hydrogen generated by the reaction is discharged into the air through the solution, and part of the hydrogen gathers at the crack tip, and then diffuses in the matrix in the form of atoms along the grain boundaries, dislocations, and other defects, as well as low energy surfaces [29], resulting in a sharp decline in the mechanical strength and ductility of the specimens in Fig. 12. The mixing mechanism of

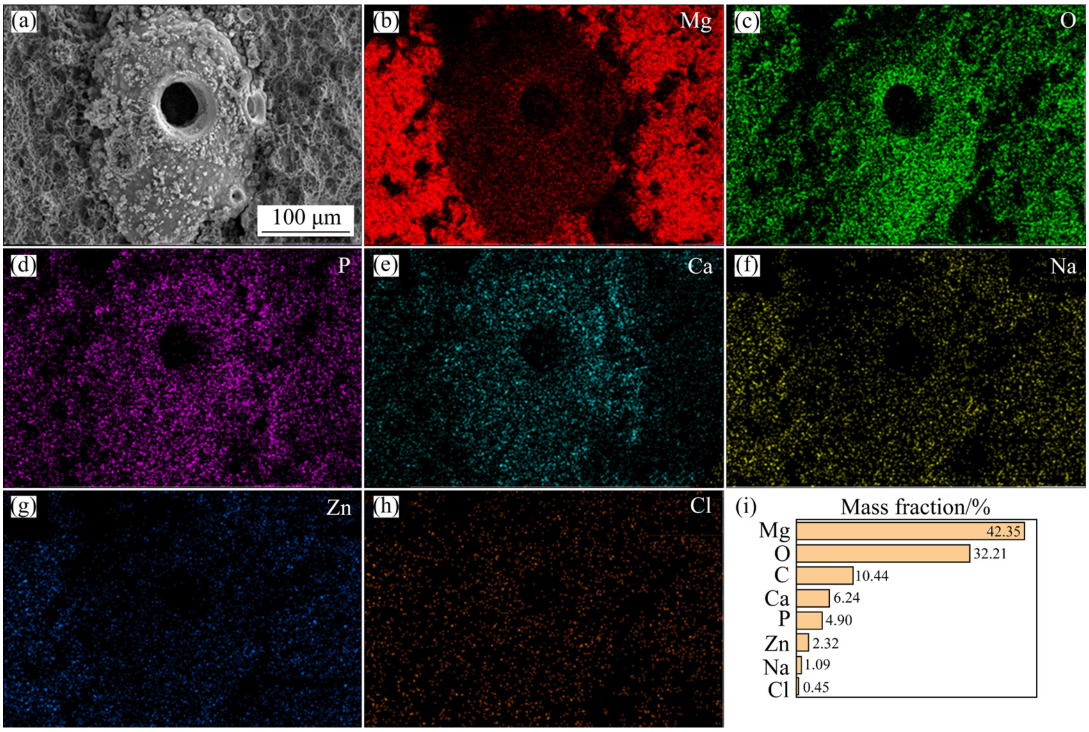

Fig. 11 Morphology (a) and element distribution (b−i) of MZC-MF specimens for SSRT in SBF

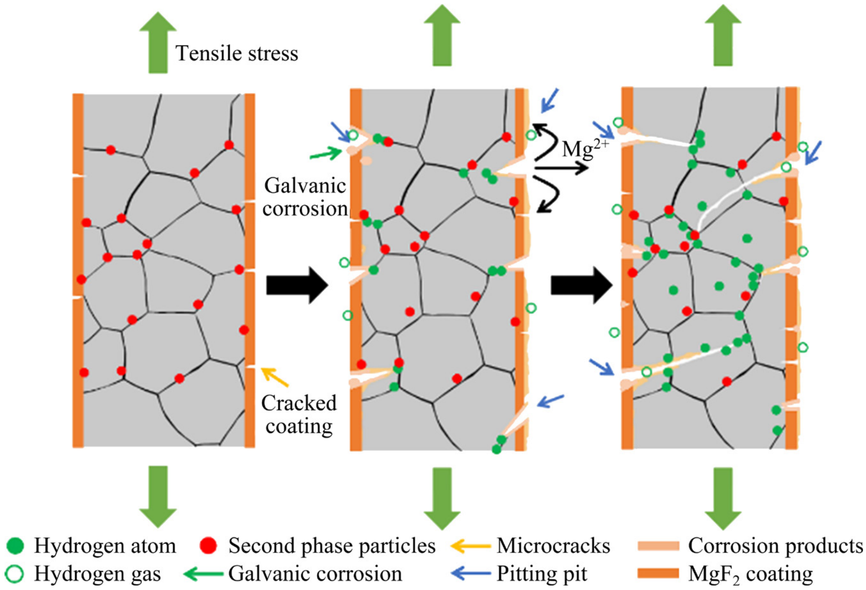

Fig. 12 Schematic diagram of SCC failure of MZC-MF specimens

anodic dissolution and hydrogen-induced cracking is the main reason for stress corrosion fracture of the MZC alloy. It is clear from the existing literature [30] that the coating does not play a key role in the crack growth stage, but its contribution is limited to the crack initiation stage.

4 Conclusions

(1) MgF2 coating could significantly improve the stress corrosion resistance of MZC alloy.

(2) MgF_2 coating could greatly reduce the stress corrosion cracking sensitivity of MZC alloy in SBF. Compared to MZC alloy, stress corrosion cracking sensitivity index (I_{scc}) of MZC-MF alloy decreased by 21% (UTS), 22% (t_f), 23% (δ), 7% (φ) and 15% (A), respectively.

(3) The coating of magnesium fluoride on the surface delayed the anodic dissolution and hydrogen-induced embrittlement.

Acknowledgments

The authors acknowledge the financial support for this work from the National Natural Science Foundation of China (Nos. U1764254, 51871166), and the Tianjin Natural Science Foundation, China (No. 20JCYBJC00620).

References

[1] CHEN Lian-xi, SHENG Yin-ying, ZHOU Han-yu, LI Zhi-bin, WANG Xiao-jian. Influence of a MAO plus PLGA coating on biocorrosion and stress corrosion cracking behavior of a magnesium alloy in a physiological environment [J]. Corrosion Science, 2019, 148: 134−143.

[2] CHOUDHARY L, RAMAN R K S. Magnesium alloys as body implants: Fracture mechanism under dynamic and static loadings in a physiological environment [J]. Acta Biomaterialia, 2012. 8: 916−923.

[3] GIANNITELLI S M, ACCOTO D, TROMBETTA M, RAINER A. Current trends in the design of scaffolds for computer-aided tissue engineering [J]. Acta Biomaterialia, 2014, 10: 580−594.

[4] GU X N, ZHOU W R, ZHENG Y F, CHENG Y, WEI S C, ZHONG S P, XI T F, CHEN L J. Corrosion fatigue behaviors of two biomedical Mg alloys−AZ91D and WE43−in simulated body fluid [J]. Acta Biomaterialia, 2010, 6: 4605−4613.

[5] KOO Y, JANG Y, YUN Y. A study of long-term static load on degradation and mechanical integrity of Mg alloys-based biodegradable metals [J]. Materials Science and Engineering B: Advanced Functional Solid-State Materials, 2017, 219: 45−54.

[6] SOZANSKA M, MOSCICKI A. Investigation of the susceptibility of the WE54 magnesium-based alloy to stress corrosion cracking [J]. Journal of Materials Engineering and Performance, 2020, 29: 949−963.

[7] JAFARI S, RAMAN R K S, DAVIES C H J. Stress corrosion cracking of an extruded magnesium alloy (ZK21) in a simulated body fluid [J]. Engineering Fracture Mechanics, 2018, 201: 47−55.

[8] SAHIN S, CEHRELI M C, YALCIN E. The influence of functional forces on the biomechanics of implant-supported prostheses—A review [J]. Journal of Dentistry, 2002, 30: 271−282.

[9] BHUIYAN M, MUTOH Y, MURAI T, IWAKAMI S. Corrosion fatigue behavior of extruded magnesium alloy AZ61 under three different corrosive environments [J]. International Journal of Fatigue, 2008, 30: 1756−1765.

[10] GONZALEZ N P, TORRES B, S. RODRIGUEZ G, RODRIGO P, BONACHE V, MANRIQUE H P, MOHEDANO M, RAMS J. Mg−1Zn−1Ca alloy for biomedical applications: Influence of the secondary phases on the mechanical and corrosion behaviour [J]. Journal of Alloys and Compounds, 2020, 831: 154735.

[11] FANG Hui, WANG Chen-xi, ZHOU Shi-cheng, ZHENG Zhen, LU Tian, LI Ge, TIAN Yan-hong, SUGA T. Enhanced adhesion and anticorrosion of silk fibroin coated biodegradable Mg−Zn−Ca alloy via a two-step plasma activation [J]. Corrosion Science, 2020, 168: 108466.

[12] DING Peng-fei, LIU Yuan-chao, HE Xiang-hui, LIU De-bao, CHEN Min-fang. In vitro and in vivo biocompatibility of Mg−Zn−Ca alloy operative clip [J]. Bioactive Materials, 2019, 4: 236−244.

[13] DUBEY D, KADALI K, PANDA S S, KUMAR A, JAIN J, MONDAL K, SINGH S S. Comparative study on the stress corrosion cracking susceptibility of AZ80 and AZ31 magnesium alloys [J]. Materials Science and Engineering A, 2020, 792: 139793.

[14] CHOUDHARY L, RAMAN R K S. Mechanical integrity of magnesium alloys in a physiological environment: Slow strain rate testing based study [J]. Engineering Fracture Mechanics, 2013, 103: 94−102.

[15] JAFARI S, HARANDI S E, RAMAN R K S. A review of stress-corrosion cracking and corrosion fatigue of magnesium alloys for biodegradable implant applications [J]. Jom, 2015, 67: 1143−1153.

[16] COOPER L, ZHOU Y, TAKEBE J, GUO J, ABRON A, HOLMEN A, ELLINGSEN J. Fluoride modification effects on osteoblast behavior and bone formation at TiO_2 grit-blasted c.p. titanium endosseous implants [J]. Biomaterials, 2006, 27: 926−936.

[17] LI Zhen, SUN Shi-zhao, CHEN Min-fang, FAHLMAN B D, LIU De-bao, BI Hong-wei. In vitro and in vivo corrosion, mechanical properties and biocompatibility evaluation of MgF_2-coated Mg−Zn−Zr alloy as cancellous screws [J]. Materials Science and Engineering C: Materials for Biological Applications, 2017, 75: 1268−1280.

[18] CHOUDHARY L, SZMERLING J, GOLDWASSER R, RAMAN R S. Investigations into stress corrosion cracking behaviour of AZ91D magnesium alloy in physiological environment [J]. Procedia Engineering, 2011, 10: 518−523.

[19] LI Hui-zhong, YAO San-cheng, LIANG Xiao-peng, CHEN Yong-hui, LIU Chao, HUANG Lan. Grain boundary pre-precipitation and its contribution to enhancement of corrosion resistance of Al−Zn−Mg alloy [J]. Transactions of Nonferrous Metals Society of China, 2016, 26: 2523−2531.

[20] GAO Yuan-ming, WANG Li-zhen, LI Lin-hao, GU Xue-nan, ZHANG Kuo, XIA Jie, FAN Yu-bo. Effect of stress on corrosion of high-purity magnesium in vitro and in vivo [J]. Acta Biomaterialia, 2019, 83: 477−486.

[21] SUN J, JIN S, ZHAO B C, CAI H, SUN L, XUAN X. Enhanced corrosion resistance of biodegradable Mg alloys via ultrasonically treated fluoride coating [J]. Surface Topography: Metrology and Properties, 2019, 7: 025009.

[22] VERDIER S, LAAK N V D, DELALANDE S, METSON J, DALARD F. The surface reactivity of a magnesium-aluminium alloy in acidic fluoride solutions studied by electrochemical techniques and XPS [J]. Applied Surface Science, 2004, 235: 513−524.

[23] DAROONPARVAR M, YAJID M A M, GUPTA R K, YUSOF N M, RAD H R B, GHANDVAR H, GHASEMI E. Antibacterial activities and corrosion behavior of novel PEO/nanostructured ZrO_2 coating on Mg alloy [J]. Transactions of Nonferrous Metals Society of China, 2018, 28: 1571−1581.

[24] PRZONDZIONO J, HADASIK E, WALKE W. Resistance to electrochemical corrosion of the extruded magnesium alloy AZ80 in NaCl solutions [J]. Materiali in Tehnologije, 2015, 49: 275−280.
[25] ZHAO Jia, YOU Chen, CHEN Min-fang, LV Shao-yuan, TIE Di, LIU Hai-feng. Effect of calcium oxide particle size on microstructure and properties of AZ91 Mg alloy [J]. Journal of Alloys and Compounds, 2021, 26: 160970.
[26] CHOUDHARY L, RAMAN R K S, HOFSTETTER J, UGGOWITZER P J. In-vitro characterization of stress corrosion cracking of aluminium-free magnesium alloys for temporary bio-implant applications [J]. Materials Science and Engineering C: Materials for Biological Applications, 2014, 42: 629−36.
[27] WALTON C A, MARTIN H J, HORSTEMEYER M F, WHITTINGTON W R, HORSTEMEYER C J, WANG P T. Corrosion stress relaxation and tensile strength effects in an extruded AZ31 magnesium alloy [J]. Corrosion Science, 2014, 80: 503−510.
[28] AMBAT R, AUNG N N, ZHOU W. Studies on the influence of chloride ion and pH on the corrosion and electrochemical behaviour of AZ91D magnesium alloy [J]. Journal of Applied Electrochemistry, 2000, 30: 865−874.
[29] ZENG Rong-chang, DIETZEL W, ZETTLER R, GAN Wei-min, SUN Xin-xin. Microstructural evolution and delayed hydride cracking of FSW-AZ31 magnesium alloy during SSRT [J]. Transactions of Nonferrous Metals Society of China, 2014, 24: 3060−3069.
[30] KANNAN M B, LIYANAARACHCHI S. Hybrid coating on a magnesium alloy for minimizing the localized degradation for load-bearing biodegradable mini-implant applications [J]. Materials Chemistry and Physics, 2013, 142: 350−354.

MgF_2 涂层对 Mg−Zn−Ca 合金在模拟体液中应力腐蚀开裂行为的影响

李育丰[1,2]，王柏文[1]，孙小淏[3]，刘德宝[4]

1. 天津理工大学 材料科学与工程学院，天津 300384；
2. 河北工业大学 材料科学与工程学院，天津 300401；
3. 光电材料与器件天津市重点实验室，天津 300384；
4. 天津理工大学 功能材料国家级实验教学示范中心，天津 300384

摘 要：采用慢应变拉伸测试方法对 Mg−3wt.%Zn−0.2wt.%Ca(质量分数)(MZC)合金和氟化镁(MgF_2)涂层 Mg−3wt.%Zn−0.2wt.%Ca 合金(MZC-MF)的应力腐蚀开裂行为进行研究。结果表明，MgF_2 涂层可以显著提高 MZC 合金在模拟体液(SBF)中的耐腐蚀性并延长其断裂失效时间。MgF_2 涂层明显降低 MZC 合金在 SBF 中的应力腐蚀敏感性，应力腐蚀开裂敏感性指数(Iscc)分别降低 21% (UTS), 22% (t_f), 23% (δ), 7% (φ)和 15% (A)。

关键词：Mg−Zn−Ca 合金；氟化镁涂层；应力腐蚀敏感性；应力腐蚀开裂；断裂失效模式

(Edited by Bing YANG)